Journal of Applied Fluid Mechanics, Vol. 13, No. 3, pp. 805-813, 2020.
Available online at www.jafmonline.net, ISSN 1735-3572, EISSN 1735-3645.
DOI: 10.29252/jafm.13.03.30717

Substitute Model and CFD Investigations of a Coalescer in a Three-Phase Crude Oil Gravity Separator

Z. Krzemianowski†, M. Lackowski, T. Ochrymiuk and P. Flaszyński

Institute of Fluid-Flow Machinery Polish Academy of Sciences, Fiszera 14, Gdańsk, 80-231, Poland

†*Corresponding Author Email: krzemian@imp.gda.pl*

(Received July 4, 2019; accepted October 12, 2019)

ABSTRACT

The flow structure in a three-phase gas-oil-water separator and its performance was the main objective of the presented investigations, for which the Euler-Euler multiphase model to simulate the flow was used. The main assumption of the model is that secondary phases, consisting of oil and water droplets, are mono-dispersed with no coalescence and breakup. The considered separator is a part of the installation operated by a drilling company. In general, the investigation of separation process is very computationally expensive and time-consuming, therefore it is desirable to search for some simplifications in order to be able to carry out engineering analysis of the processes taking place in a separator. Hence, the three-dimensional coalescer was investigated as a porous element in order to find pressure losses dependence on flow velocity, which was required to simulate the existence of coalescers and baffles. As the next step, a transient Eulerian multiphase simulations were carried out for gas-oil-water mixture in a real horizontal gravity separator for two- and three-dimensional case. Required data for calculations was derived from real exploration well. In the two-dimensional case, the worked out dependence of the pressure drop with respect to velocity was used to model the flow through the porous coalescers. In three-dimensional case, the coalescers and baffles were modelled without any simplifications. It was found that general trends can be predicted despite the simplification of the geometrical model in which coalescer and baffle geometries have been replaced by a porous medium. The calculations confirmed that the complexity of geometry requiring time-consuming calculations can be usually replaced by introducing simplifications allowing for engineering analysis of separator operation that is acceptable by the industry, because the basic parameters regarding the separation process can be determined.

Keywords: Oil separators; Multiphase calculations; Coalescers.

NOMENCLATURE

b	body force
C_2	internal resistance coefficient
$\bar{\bar{d}}$	deformation velocity tensor
e	sum of internal and kinetic energy
$\bar{\bar{I}}$	unit tensor
p	pressure
q	molecular heat flux
q_t	turbulent heat flux
q_{dif}	diffusion heat flux
q_{rad}	radiation heat flux
$\bar{\bar{r}}$	Reynolds turbulent flux tensor
$\bar{\bar{t}}$	momentum flux tensor
v	velocity
Δp	pressure drop
α	permeability
ϵ	internal energy
μ	molecular dynamic viscosity
ρ	density
$\bar{\bar{\tau}}$	shear stress tensor
$\bar{\bar{\tau}}^{dif}$	diffusion momentum flux tensor
$\bar{\bar{\tau}}^{rad}$	radiation momentum flux tensor
$\bar{\bar{\tau}}^{trans}$	transpiration momentum flux tensor

1. INTRODUCTION

The well-known phenomenon of gravity is effectively used in oil and gas industry for separation of water and air from oil-mixture flow. Typical geometry of horizontal gravity separators is a

cylindrical vessel characterized by high aspect ratio and short entrance zone for separation of gas and liquid. Improvement of separation effectiveness can be achieved by implementation of various devices inside the vessel: vanes or momentum breakers, plates, baffles (perforated or solid), flow straighteners, mist eliminators, foam breakers, coalescers. All of them improve the effectiveness of a separation process.

Due to the complex flow in the three-phase separator, the mathematical assumption of design is usually based on semi-empirical formula derived from Stokes law (Arnold & Stewart, 2008). The formula for the settling velocity contains some correction coefficients dependent on the separator configuration (Svrcek & Monnery, 1993, Kharoua *et al.* 2010). Other authors emphasize several complex phenomena such as liquid re-entrainment (Viles 1992), recirculation within the liquid layers (Hansen & Rørtveit, 2006), and foaming (Shaban 1995) or dispersion of emulsion zone between water and oil layers (Arntzen & Andersen, 2001).

Numerical methods, widely recognized as Computational Fluid Dynamics (CFD), are considered as effective tool used at the separator design stage. CFD can also be successfully applied to improve the separation effectiveness. As already presented by Hansen *et al.* (1991), three-phase separator can be modelled assuming the existence of two-phase regions inside: a zone with liquid droplets dispersed in gas and the liquid bath with oil or water droplets dispersed in liquid. The emulsion viscosity was modelled by modification of the oil viscosity with the local water volume fraction. From other hand (Yayla *et al.* 2019) two-phase three-dimensional turbulent flow simulations are carried out by applying of Euler mixture model and effects of the location. The influence of distance between the inlet of the separator and the diverter plate and inlet velocity on the separation efficiency are also investigated. One can mention another approach proposed by Laleh *et al.* (2012), in which the oil-water emulsion was modelled as a mixture by means of the volume of fluid method and the water separation efficiency was determined by tracking a droplet distribution with an uncoupled Lagrange dilute-phase particle tracking model.

Development of appropriate models taking into account the droplet size distribution together with coalescence and breakup phenomena was presented by Song *et al.* (2010), Grimesa (2012) and Grimesa *et al.* (2012). The effects of selected parameters on the separator effectiveness and internal flow was investigated by Abdulkadir and Perez (2010), Vilagines and Akhras (2010), Liang *et al.* (2013) and Kharoua *et al.* (2013). Due to the complexity of the multiphase flow in horizontal gravity separators, a parametric CFD study allows for the assessment of the parameters sensitivity (Abdulkadir & Perez 2010, Kharoua *et al.* 2013) and model simplification while the obtained results are still kept on the acceptable level of accuracy. In general, the multiphase flow was usually modelled as a two-phase flow only, which combined with two-equation turbulence model provided robust approach allowing for simulations at a reasonable computational cost. One can mention an experimental study and a parallel numerical simulation concerning a three-dimensional turbulent flow of air in a cyclone separator (Talbi *et al.* 2011). The obtained results show interesting effects such as the three-dimensional nature of flow behavior, which should not be ignored in the initial design process.

In the sense of a physical model, for the purpose of two-dimensional CFD calculations (due to model constraints), it seems reasonable that coalescers and baffles most preferably should be treated as a porous material, because in this case it is not possible to map their full three-dimensional geometry. A mathematical model and calculations of the flow resistance concerning the flow in the coalescer are presented below. To determine the coalescer resistance, three-dimensional calculations were first made to determine the porosity coefficients. Then, the results for the two-dimensional separator are presented, in which the coalescers and baffles were modeled as a porous material. The last part presents the three-dimensional flow calculations in the separator in which the coalescers and baffles are fully modelled without any simplifications. Data for calculations was based on real data from the exploration well, courtesy of the drilling company.

2. CALCULATIONS OF FLOW RESISTANCE IN A COALESCER

As mentioned in the introduction, in order to perform two-dimensional calculations of the separator, first calculations of a three-dimensional coalescer were first made to determine the coefficients allowing to determine the porous material replacing the actual coalescers and baffles. For this purpose, a computational model of single-phase flow through coalescing channels was built and a series of three-dimensional calculations were carried out with different flow velocities to determine the pressure drops in the coalescer.

2.1 Geometrical Model and Boundary Conditions

The geometry and the computational mesh are shown in Fig. 1 and in Fig. 2, respectively. The inlet boundary condition was defined as a uniform velocity with turbulence intensity and turbulent viscosity ratio defined as 5 and 10% respectively (these boundary conditions were based on the experiences on similar flow configurations), for all considered mass flow rates. The complete geometry of the coalescer was modelled using periodic boundary conditions. For meshing of this configuration in three-dimensional approach a total amount of $3.15 \cdot 10^5$ elements were used. Good mesh quality was expressed by the value of minimum orthogonal quality, which did not exceed 0.26. Value of maximum aspect ratio of cells was 8.60. For this mesh, the maximum values of Y^+ on the walls did not exceed 0.8 for the maximum flow rate.

2.2 Mathematical Model

When designing the separator using zero-

dimensional models, the basic parameters of the separator are obtained, which can then be optimized using advanced three-dimensional methods such as CFD techniques. Due to the geometric complexity and the scale of physical phenomena, before the final three-dimensional design cycle, it is reasonable to build computational surrogate model of the most important components of the separator such as coalescer, demister or deflector. It is based on mass, momentum and energy conservation equations presented below.

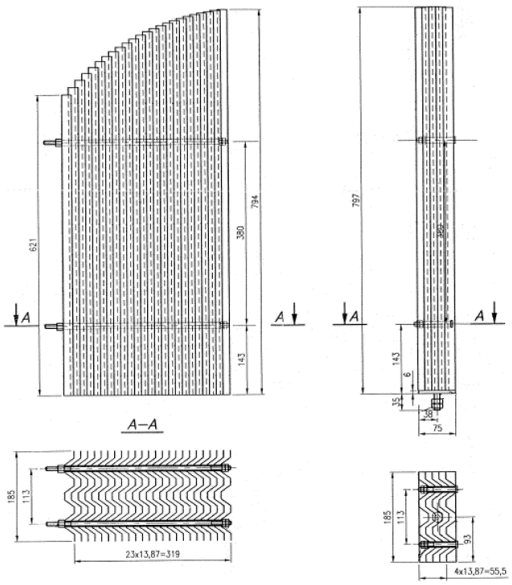

Fig. 1. A general view of side and middle part of the separator coalescer.

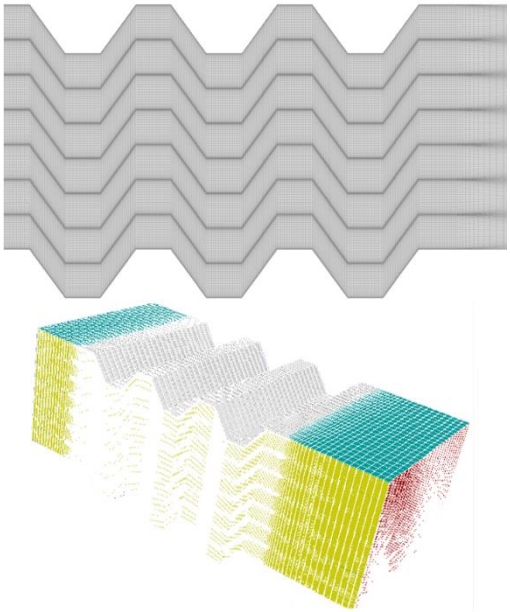

Fig. 2. Computational mesh of the three-dimensional coalescer model.

The continuity equation can be written in the following form:

$$\frac{\partial}{\partial t}\rho + \nabla \cdot (\rho \vec{v}) = 0 \tag{1}$$

where ρ is the density, v is the velocity vector.

From Eq. (1) it follows that the density becomes the basic variable of the numerical model. The basic vector of conservative variables will be as follows:

$$U = \{\rho, \rho\vec{v}, \rho\epsilon\} \tag{2}$$

which specifies conservative variables (the unknowns in the equations) and in which ϵ is the internal energy.

Let us assume that the momentum flux $\bar{\bar{t}}$ contains a reversible part in the form of thermodynamic pressure p and a number of dissipative parts, among which the flux of shear stresses $\bar{\bar{\tau}}$ and Reynolds turbulent flux $\bar{\bar{r}}$ belong to the most important ones:

$$\bar{\bar{t}} = -p\bar{\bar{I}} + \bar{\bar{\tau}} + \bar{\bar{r}} + \bar{\bar{\tau}}^{dif} + \bar{\bar{\tau}}^{rad} + \bar{\bar{\tau}}^{trans} =$$
$$= -p\bar{\bar{I}} + \bar{\bar{\tau}}^{total} \tag{3}$$

where $\bar{\bar{I}}$ is the unit tensor.

The remaining contributions to the momentum flux include: diffusion $\bar{\bar{\tau}}^{dif}$, radiation $\bar{\bar{\tau}}^{rad}$ and transpiration $\bar{\bar{\tau}}^{trans}$. Dividing the fluxes into the convective part (first order derivatives) and the diffusion part (second order derivatives), the evolution of the momentum is written down in the following conservative form:

$$\frac{\partial}{\partial t}(\rho\vec{v}) + div\left(\rho\,\vec{v}\,\vec{v} + p\bar{\bar{I}}\right) = div(\bar{\bar{\tau}}^{total}) + \rho\vec{b} \tag{4}$$

where $\vec{b}$ is the body forces vector. In Cartesian coordinates it can be written down as:

$$\frac{\partial}{\partial t}(\rho v_i) + \frac{\partial}{\partial x_j}\left(\rho v_i v_j + p\delta_{ij}\right) =$$
$$= div(\bar{\bar{\tau}}^{total}) + \rho b_i \tag{5}$$

It results from the above equations of the momentum balance that the "stress" boundary condition, imposed on the total momentum flux, can take the following form:

$$\vec{\tau}^{a} = \bar{\bar{t}}\vec{n} \tag{6}$$

where $\vec{\tau}^{a}$ is the vector of given surface forces, which in a particular case can be equal to a given pressure, $\vec{\tau}^{a} = p^{a}\vec{n}$, where $\vec{n}$ is the unit vector normal to a surface.

Since we assume that all fluid components have the same velocity $\vec{v}$ and the same spatial gradients, the expected formula for tensor of viscous stresses is the Stokes formula:

$$\bar{\bar{\tau}} = 2\mu\left[\bar{\bar{d}} - \frac{1}{3}\nabla\cdot(\vec{v})\bar{\bar{I}}\right] + \mu'\,\nabla\cdot(\vec{v})\bar{\bar{I}} \tag{7}$$

in which $\bar{\bar{d}}$ is the deformation velocity tensor:

$$\bar{\bar{d}} = \frac{1}{2}(\nabla\vec{v} + \vec{v}\nabla) = \frac{1}{2}\left(\frac{\partial v_i}{\partial x_j} + \frac{\partial v_j}{\partial x_i}\right)\vec{e_i}\,\vec{e_j} = d_{ij}\,\vec{e_i}\,\vec{e_j} \tag{8}$$

and in which μ is the dynamic viscosity, μ' is the second viscosity coefficient usually equal to zero.

Transport equations required for the k-ε turbulence model:

$$\frac{\partial}{\partial t}(\rho k) = \nabla \cdot (\rho k \vec{v}) = \nabla \cdot \left(\frac{\mu_t}{\sigma_k} \nabla k\right) + S_k \quad (9)$$

$$\frac{\partial}{\partial t}(\rho \varepsilon) = \nabla \cdot (\rho \varepsilon \vec{v}) = \nabla \cdot \left(\frac{\mu_t}{\sigma_\varepsilon} \nabla \varepsilon\right) + S_\varepsilon \quad (10)$$

have the same conservative form as other transport equations.

However, the source terms S_k and S_ε are not only dependent on the vector of conservative variables, but also on their spatial gradients.

Five constants of the *k*-ε model, i.e. $\sigma_k = 1.0$, $\sigma_\varepsilon = 1.3$, $C_\mu = 0.09$, $C_1 = 1.44$, $C_2 = 1.92$, do not depend on the type of flow (stationary, non-stationary) or the type of fluid (incompressible, compressible).

Equation of the total energy balance in a homogeneous fluid model consists of temporal changes of a balanced quantity, fluxes of this quantity outflowing from/inflowing to the control area and source terms:

$$\frac{\partial}{\partial t}(\rho e) + \nabla \cdot (\rho e \vec{v}) = \nabla \cdot \left(\vec{q} + \overrightarrow{q_t} + \bar{\bar{t}} \cdot \vec{v} + \overrightarrow{q_{dif}} + \overrightarrow{q_{rad}}\right) + \rho r + \rho \vec{b} \cdot \vec{v} \quad (11)$$

where e is the sum of internal and kinetic energy ($e = \epsilon + \vec{v}^2/2$), $\vec{q}$ and $\overrightarrow{q_t}$ are the molecular and turbulent heat fluxes, $\bar{\bar{t}} \cdot \vec{v}$ is the mechanical heat flux, $\overrightarrow{q_{dif}}$ and $\overrightarrow{q_{rad}}$ are respectively the diffusion and radiation heat fluxes.

Because the total momentum flux is divided into a convective reversible part ($p\,\bar{\bar{I}}$) and a mechanical diffusion part, so the mechanical momentum flux term: $-p\,\bar{\bar{I}} \cdot \vec{v} = -p\vec{v}$ can be transferred to the left hand side:

$$\frac{\partial}{\partial t}(\rho e) + \nabla \cdot \left[\left(\epsilon + \frac{p}{\rho}\right)\rho \vec{v}\right] =$$

$$= \nabla \cdot \left(\vec{q} + \overrightarrow{q_t} + \bar{\bar{\tau}}^{total} \cdot \vec{v} + \overrightarrow{q_{dif}} + \overrightarrow{q_{rad}}\right) + S_e \quad (12)$$

For the enthalpy h formulation, the following relation should be used:

$$\rho e = \rho h + \rho \frac{\vec{v}^2}{2} - p \quad (13)$$

where

$$h = \epsilon + \frac{p}{\rho} \quad (14)$$

is the enthalpy related to the mass unit.

The porous medium is described by the source term S_i added to the standard momentum equation:

$$\frac{\partial}{\partial t}(\rho \vec{v}) + \nabla \cdot (\rho \vec{v} \vec{v}) =$$

$$= -\nabla \mathrm{p} + \nabla \cdot (\bar{\bar{\tau}}) + p\vec{g} + \vec{S} \quad (15)$$

and

$$\bar{\bar{\tau}} = \mu \left[(\nabla \vec{v} + \nabla \vec{v}^T) - \frac{2}{3} \nabla \cdot \vec{v}\,\bar{\bar{I}}\right] \quad (16)$$

The term S_i is the source term of the momentum conservation equation ($i = x, y, z$) and consists of two parts: viscous losses due to the flow resistance of a porous medium (Darcy's law, the first term of the right hand side of the Eq. (17)) and internal losses (the second term of the right hand side of the Eq. (17)):

$$S_i = -\left(\sum_{j=1}^{3} D_{ij}\, \mu\, v_j + \sum_{j=1}^{3} C_{ij} \frac{1}{2} \rho |v| v_j\right) \quad (17)$$

where $|v|$ is the velocity magnitude and D and C are the given matrices. The momentum loss is related to the pressure gradient in the porous medium and results in a pressure drop proportional to the flow velocity. In the case of homogeneous porous materials, we have:

$$S_i = -\left(\underbrace{\frac{\mu}{\alpha} v_i}_{viscous\ loss} + \underbrace{C_2 \frac{1}{2} \rho |v| v_i}_{internal\ loss}\right) \quad (18)$$

where α is permeability, and C_2 is the coefficient of internal resistance, i.e. D and C are the diagonal matrices with $1/\alpha$ and C_2, respectively on diagonals and zeros for the rest of matrix elements.

In laminar flows through porous materials, the pressure drop is directly proportional to the velocity and the C_2 constant can be omitted. Neglecting convective and diffusion phenomena, the flow model in porous materials is reduced to Darcy's law:

$$\nabla p = -\frac{\mu}{\alpha} \vec{v} \quad (19)$$

The pressure drop is calculated for an each direction (x, y, z) of a porous medium as follows:

$$\Delta p_x = \sum_{j=1}^{3} \frac{\mu}{\alpha_{xj}} v_j\, \Delta n_x \quad (20a)$$

$$\Delta p_y = \sum_{j=1}^{3} \frac{\mu}{\alpha_{yj}} v_j\, \Delta n_y \quad (20b)$$

$$\Delta p_z = \sum_{j=1}^{3} \frac{\mu}{\alpha_{zj}} v_j\, \Delta n_z \quad (20c)$$

where $1/\alpha_{ij}$ are the components of matrix D, v_j are the components of velocity in the x, y, z directions, and Δn_x, Δn_y, Δn_z are the thicknesses of a porous medium in the x, y, z directions.

At higher flow velocities the C_2 constant introduces correction for losses generated by internal resistance. This constant can be interpreted as the loss factor proportional to the length along the flow direction.

In the case of perforated plates (substituted by a porous material), it is possible to omit the permeable term and use only the internal losses term, which finally takes the form:

$$\Delta p_i = -\sum_{j=1}^{3} C_{2\,ij} \left(\frac{1}{2} \rho v_j |v|\right) \quad (21)$$

That can be written down as pressure drops in the x, y, z directions:

$$\Delta p_x \approx \sum_{j=1}^{3} C_{2\,xj}\, \Delta n_x \frac{1}{2} \rho v_j |v| \quad (22a)$$

$$\Delta p_y \approx \sum_{j=1}^{3} C_{2\,yj}\, \Delta n_y \frac{1}{2} \rho v_j |v| \quad (22b)$$

$$\Delta p_z \approx \sum_{j=1}^{3} C_{2\,zj}\, \Delta n_z \frac{1}{2} \rho v_j |v| \quad (22c)$$

The essence of replacing the perforated plates with a porous material is to determine the characteristics of a substitute porous material. In the CFD code, a porous medium is described by three parameters – expressed by one scalar and two vectors. The scalar

is the porosity of a medium, i.e. the ratio of the hole areas to the total surface of a plate in the case of perforated plate. The vectors are the permeability α and the internal resistance coefficient C_2.

To evaluate α and C_2 it is necessary to determine the so-called characteristics of the substitute porous medium, i.e. pressure drop on the perforated plate as a function of the flow velocity.

For this purpose Eq. (18) is used, because the source term has the meaning of an additional pressure drop generated by a perforated plate divided by the thickness of a plate, i.e.:

$$\frac{\Delta p}{\Delta l} = \frac{\mu}{\alpha} v + C_2 \frac{1}{2} \rho v^2 \tag{23}$$

As the result of the calculations the dependence of pressure loss in the flow through the coalescer with respect to inflow velocity was determined. The results are presented in the next subsection.

2.3 Results of Three-Dimensional Flow Calculations in a Coalescer

The following Fig. 3 presents the results of numerical simulation of the coalescence resistance characteristics (inflow velocity v vs. pressure loss Δp). Basing on this diagram, the parameters of the porous medium (using Eq. (25)) α and C_2 were obtained (by interpolating data by means of the quadratic function). These results were used next to model coalescers and baffles of the separator as porous media in two-dimensional calculations.

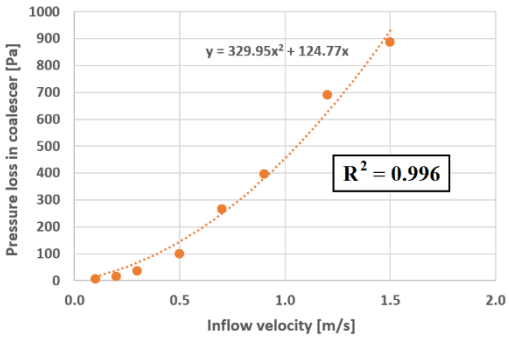

Fig. 3. Coalescer characteristics (inflow velocity vs. pressure loss) obtained as a result of numerical investigations.

3. Two-Dimensional Case Of A Separator

3.1 Geometrical Model

The schematic of the two-dimensional separator used in CFD calculations is shown in Fig. 4. The characteristic dimensions were as follows: length 3 m, height 1 m, oil-water-gas mixture inlet diameter 0.1 m, oil and water fractions outlet diameters 0.08 m, gas fraction outlet diameter 0.15 m, width of a single coalescer 0.2 m, width of a single baffle 0.003 m. An example of a computational grid is shown in Fig. 5 for the inlet and outlet regions.

Two-dimensional calculations required the simplifications in the geometric model, since the actual shapes of coalescers and baffles in such case are not modelable. Therefore, two coalescers and two baffles placed in the separator were modelled as porous elements.

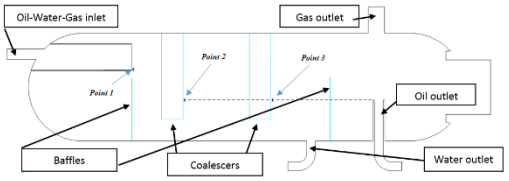

Fig. 4. Geometrical model of the separator.

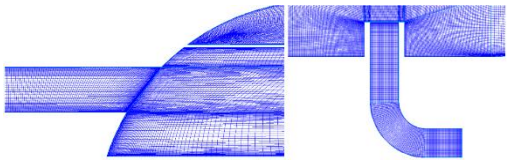

Fig. 5. Views of the computational mesh at inlet part (left) and oil outlet part of the separator (right).

3.2 Boundary Conditions and Model Parameters

The boundary conditions used in the carried out two-dimensional numerical transient calculations are described below. Because the turbulent flow was stated (with the lowest Reynolds number ~16000), so as a closure of conservation equations, two-equation RANS (Reynolds Averaged Navier-Stokes) k-ε Standard turbulence model with the Standard Wall Functions was used. The selection of this turbulence model was due to its robustness, low mesh requirements ($Y^+ > 30$) and relatively low computational needs, which is very beneficial in the case of three-phase separator calculations. The number of computational grid elements was approximately $270 \cdot 10^3$ of quadrilateral cells.

The basic parameters used in the calculations were assumed as follows: multiphase approach of the Eulerian type (number of fractions 3); primary/secondary fractions: gas – primary, water – secondary, oil – secondary; droplet liquid diameters (oil and water) 0.0001 m; volumetric flow rate of the mixture at inlet: 12.5 m^3/h (velocity: 0.442 m/s) and 50 m^3/h (velocity: 1.768 m/s); turbulence: hydraulic diameter at mixture inlet 0.1 m, hydraulic diameter at gas outlet 0.15 m (oil and water outlets were closed), turbulence intensity at inlet and outlet 2% (this is relatively small value due to the relatively small turbulent Reynolds numbers and existing long inflow and outflow pipelines straightening the flow). The additional boundary conditions are presented in Table 1.

As already mentioned, the porosity in the conservation equations is taken into account by source terms of the momentum S_i (where i denotes the directions x, y) – see Eq. (18), added to conservation equations, defining viscous resistance and internal losses, respectively. In the presented case the changes of parameters in the x direction

Table 1 General boundary conditions applied in calculations of separator (denotations: G – gas, W – water, O – oil)

Volume fractions at inlet, %			Density, kg·m^{-3}			Dynamic viscosity, kg·m^{-1}·s^{-1}			Surface tension, N·m^{-1}		
G	W	O	G	W	O	G	W	O	G-W	O-G	W-O
47	3	50	17.6	999.1	813.5	0.000011	0.0011	0.0023	0.072	0.034	0.05

Table 2 Specific boundary conditions applied in calculations of resistance parameters for coalescers and baffles

Flow direction	Inverse of permeability - resistivity ($1/\alpha$), m^{-1}			Coefficient of internal resistance (C_2), m^{-2}		
	Gas	Water	Oil	Gas	Water	Oil
Baffles						
x	142857	142857	142857	15000	15000	15000
y	0	0	0	0	0	0
Coalescers						
x	5.671364e+07	537801	274823	187	3.29	4.04
y	0	0	0	0	0	0

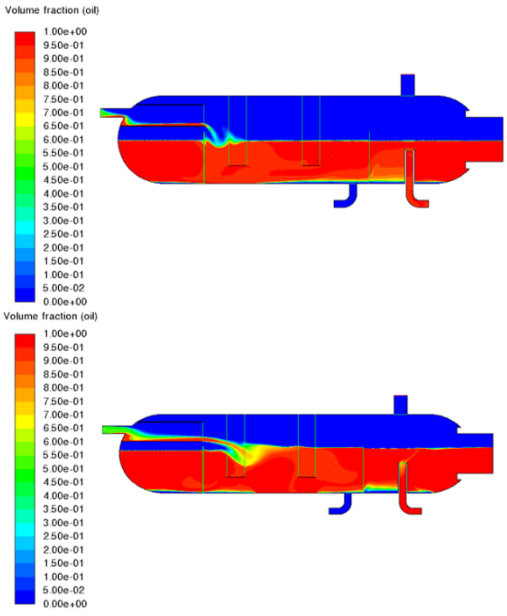

Fig. 6. Oil volume fraction (oil outlet closed): flow rate 12.5 m^3/h (upper view) – time: 60th s and 50 m^3/h (lower view) – time: 10th s.

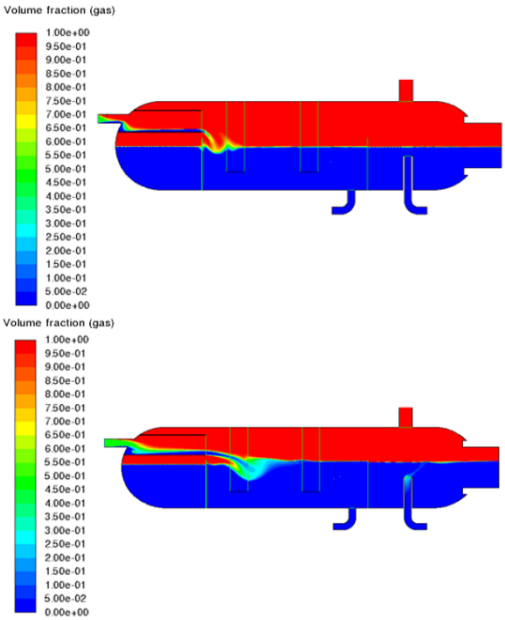

Fig. 7. Gas volume fraction (oil outlet closed): flow rate 12.5 m^3/h (upper view) – time: 60th s and 50 m^3/h (lower view) – time: 10th s.

(horizontal) only was assumed – Table 2. The changes in the *y* direction (vertical) was neglected. The porosities for coalescers and baffles were calculated as 0.9 and 0.1, respectively.

3.3 Calculations

The calculations were performed using the three-dimensional transient RANS model. The solver settings were as follows: 21.5 mm water layer from the bottom, oil layer over water up to the edge of the oil outlet pipe; the remaining area of the separator filled with the gas fraction; time step 0.005 s; pressure-velocity coupled scheme; Courant number 0.5; analysis time 60 s.

As a result of calculation for a lower flow rate, a flow image was obtained (Fig. 6 and Fig. 7) in which the mixture flowing out of the inlet part (deflector) falls down immediately into the container without reaching the coalescer. This is not the case with a larger flow rate - there the mixture jet intersects the coalescer. However, it is characteristic for both cases that the second coalescer does not affect the flow in the separator. In the case of baffles, it can be seen that they cause damming of the oil fraction, reducing the kinetic energy of the flow, thus accelerating the coalescence of all fractions.

In the inlet part of the separator, the liquid and gas fractions are intensively separated – this is particularly evident for a lower of the two flow rates considered. After leaving the inlet part, the liquid

fractions tend to disperse due to rapid falling down into the main volume of the separator. This is an undesirable phenomenon, because in the coalescer the mixture is first slowed down, which manifests itself in the dispersion of the mixture – followed by the proper separation process. This is the advantage of two-dimensional models over one-dimensional ones, because they help to diagnose such types of unfavorable phenomena.

Figures 8 and 9 show the distribution of oil fraction separation with respect to time (speed of separation) at points 1, 2, and 3 (see Fig. 4). It can be seen that for a lower flow rate the fraction change ends practically after 10 seconds. After this time the fraction changes are negligible. In the case of a larger flow rate, much higher fluctuations in the separation rate are visible, which gradually decrease over time - after more than 25 seconds the fluctuation of the separation rate has also been observed.

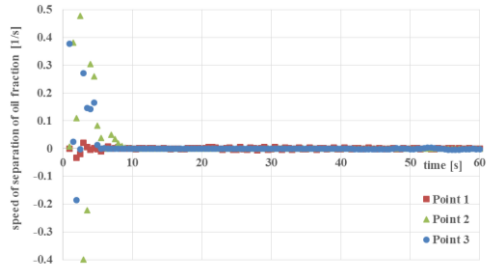

Fig. 8. Speed of separation of oil volume fraction for flow rate 12.5 m^3/h in three chosen points of a separator.

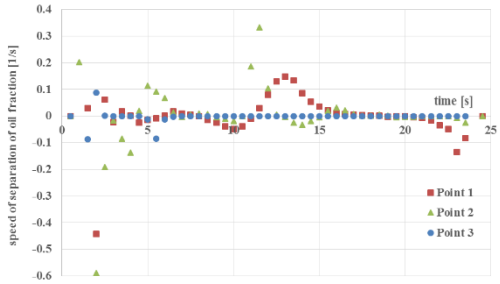

Fig. 9. Speed of separation of oil volume fraction for flow rate 50 m^3/h in three chosen points of a separator.

After using a substitute porous material with a given hydrodynamic characteristics, it is possible to create simple and fast two-dimensional models that complement pre-design balance tools like one-dimensional models and significantly improve the level of engineering design at reduced computational time. Using these methods, it is possible to redesign the separator in the realistic time desired by industry in terms of the required mass flows. With pre-designed geometry, dimensions and location of coalescers, it is also desirable to perform verification by calculations with the use of a full three-dimensional separator geometry. These calculations are, as a rule, non-stationary, very expensive and are not suitable for engineering design but they are recommended to use to check the correctness of assumptions resulting from one- and two-dimensional models.

4. THREE-DIMENSIONAL CASE OF A SEPARATOR

A non-stationary three-dimensional calculation of flow phenomena in the separator is extremely computationally expensive and time-consuming. However, in cases of new design solutions, they seem to be necessary. Therefore, calculations of the separator with full three-dimensional geometry were performed. In this case, the coalescers and baffles were modelled without any simplifications.

The boundary conditions applied to calculations were the same as for case of the two-dimensional separator (see Table 1). Regarding the volumetric flow rates of the gas-oil-water mixture 50 m^3/h (velocity 1.768 m/s) and 150 m^3/h (velocity 5.304 m/s) were applied. First of these values was indicated by manufacturer as optimal. The total amount of ~13 M mesh elements were used. Calculations were carried out in symmetry (a half of the separator).

The distribution of oil fraction contours in the separator inlet area (behind deflector) is shown in Fig. 10 for a lower flow rate (50 m^3/h). The left view shows the contours distribution of the oil fraction at the near beginning of the separation process (0.5 s), while the right view shows distribution at the time of 30 seconds. The separation process bypasses the coalescer, which makes it slower. Therefore, it can be seen that the geometry of the coalescer is not fully optimized. It is clearly visible that the assumed separation performance is achieved only at the lower part of the coalescer, where the separation process takes place most intensively. Thus, the flow rate (50 m^3/h) at which the separator operates is not optimal for its geometry.

Analogously, in the Fig. 11 (views are shown for the same times as in case of a lower flow rate) the distribution of oil fraction contours in the separator inlet area for a larger flow rate (150 m^3/h) is presented. In this case, the mixture flows through the coalescer with a much greater intensity of separation at the same moment of time as in the previous case (the separation process takes place in the frontal area of the lamellas). It results from the assumed work point, characterized by larger mass flow rates.

The separation process is strictly dependent on whether the mixture flowing out of the deflector reaches the coalescer or falls down into the separator. Hence, during the design process the key element seems to be the proper choice of the flow rates, at which the gas-water-oil mixture will drop to the coalescer. This is the crucial issue for optimal separator operation. When this is the case, the separation process becomes very intense - Fig. 11. It is clearly visible that at the very beginning of the coalescer inlet, separation zones with a pure oil fraction quickly appear.

The results of the calculations presented here in a qualitative manner are in line with expectations. A full analysis of physical phenomena occurring in the

separator allows to optimize the distribution of the main internal elements i.e. coalescers, baffles, etc. However, due to the time-consuming and costly calculations, it is recommended to perform such calculations only at the optimum work point. The full characteristics of the separator is possible to achieve in realistic time only by means of two-dimensional methods. The fraction distributions shown here fully meet the expectations of the industry and are consistent with the measurement methods installed on real objects.

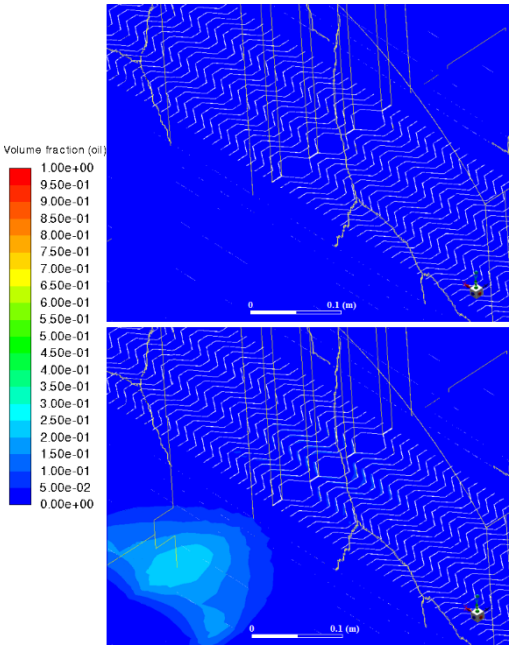

Fig. 10. Oil fraction contours in separator coalescer for flow rate 50 m^3/h in 0.5th s (upper view) and in 30th s (lower view).

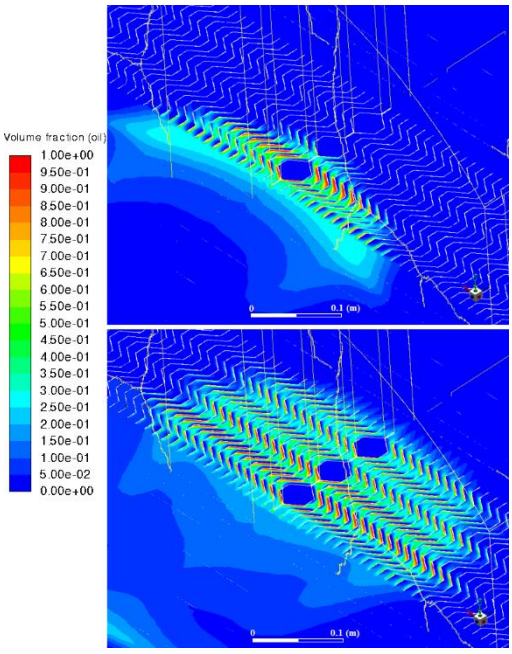

Fig. 11. Oil fraction contours in separator coalescer for flow rate 150 m^3/h in 0.5th s (upper view) and in 30th s (lower view).

5. RESULTS AND DISCUSSION

The paper attempts to synthesize preliminary design methods based on engineering balance models (one-dimensional and two-dimensional) by reducing/eliminating computationally time-consuming devices (from the calculations point of view) and substitute them with the determined hydrodynamic characteristics.

The main goal of the paper was to examine the possibilities of engineering modelling of a horizontal three-phase gravity separator devices such as coalescer, by means of simplified methods, which in turn allow the engineer to analyse the work of the separator more quickly. Therefore, a mathematical model was presented and calculations were made based on which the coalescer characteristics were determined. The obtained characteristics is the quadratic dependence of the pressure drop with respect to inflow velocity. Thanks to this, it was possible to model the coalescer as a porous geometry. Subsequently, this allowed for simplified non-stationary two-dimensional analysis of the gravity three-phase separator with the gas-water-oil mixture by means of CFD using unsteady RANS model (boundary conditions for calculations were based on physical data from the exploration well). Such an analysis is necessary to determine the correctness of the mixture flow rate selection. The results show that separation process is relatively very quick and after a few seconds the speed of separation disappears (provided that the mixture reaches the coalescer) due to the formation of a pure oil fraction.

A full non-stationary three-dimensional analysis was also carried out on one specified design assumption of the separator, using selected multiphase models. These calculations focused on the analysis of the physical process of separation as a function of flow rates being of interest to the oil industry. As a result of calculations for a lower flow rate (indicated by manufacturer as optimal) a flow field was obtained in which the mixture flowing out of the inlet part (deflector) flows immediately to the tank not reaching the coalescer. It is different in the case of the higher flow rate value - there the falling stream flows through the coalescer being dissipated inside. However, it is characteristic for both cases that the second coalescer has no influence on the flow in the separator. This indicates that the geometry of the separator is not appropriate for operating under optimal conditions and separator should be re-designed.

Designing the separator with zero-dimensional models (balance methods) the basic separator parameters can be determined. Then, they can be optimized using advanced three-dimensional methods in a way proposed here. Due to the complexity of the geometry and physical phenomena, it is reasonable to build the computational submodels of the most important separator components such as coalescer, demister or diverter, which significantly reduce the work load before the final three-dimensional design stage.

ACKNOWLEDGEMENTS

Authors specially wish to thank the Exalo Drilling S. A. (Poland) and the Computer & Measurement Co. Tercja (Gdańsk, Poland) for substantive support.

This work was supported by the (Polish) National Centre for Research & Development (NCBR) under national grant POIR.01.01.01-00-0780/15.

Some parts of CFD computations were carried out using PL-Grid Infrastructure.

REFERENCES

Abdulkadir, M. and V. H. Perez (2010). The effect of mixture velocity and droplet diameter on oil-water separator using computational fluid dynamics (CFD). *World Academy of Science Engineering and Technology* 61, 35-43.

Arnold, K. and M. Stewart (2008). Surface production operations, Vol. 1: 3rd Edition, *Design of oil-handling systems and facilities*. Gulf Professional Publishing, USA.

Arntzen, R. and P. A. K. Andresen (2001). Three-phase well-stream gravity separation. In: Johan Sjöblom, editor, *Emulsion encyclopedia*. Marcel Dekker Inc., New York, USA,

Grimesa, B. A. (2012). Population balance model for batch gravity separation of crude oil and water emulsions. Part I: Model formulation. *Journal of Dispersion Science and Technology* 33, 578-590.

Grimesa, B. A., C. A. Doraob, N. V. D. T. Opedala, I. Kralovaa, G.H. Sørlandc, and J. Sjöbloma (2012). Population balance model for batch gravity separation of crude oil and water emulsions. Part II: Comparison to experimental crude oil separation data. *Journal of Dispersion Science and Technology* 33, 591-598.

Hansen, E. W. M. and G. J. Rørtveit (2006), Numerical simulation of fluid mechanisms and separation behavior in offshore gravity separators. *Emulsions and emulsion stability: Surfactant Science Series/61*. Trondheim, Norway. CRC Press.

Hansen, E. W. M., H. Heitmann, B. Lakså, A. Ellingsen, O. Østby, T.B. Morrow, and F.T. Dodge (1991). Fluid flow modeling of gravity separators. *5th International Conference on Multi-Phase Production*, Cannes, France.

Kharoua, N., L. Khezzar and H. Saadawi (2013). CFD modelling of a horizontal three-phase separator: A Population Balance Approach. *American Journal of Fluid Dynamics* 3(4), 101-118.

Kharoua, N., L. Khezzar, and Z. Nemouchi (2010). Hydrocyclones for de-oiling applications – a review. *Petroleum Science and Technology* 28(7), 738-755.

Laleh, A. P., W. Y. Svrcek, and W. D. Monnery (2012). Design and CFD studies of multiphase separators – a review. *The Canadian Journal of Chemical Engineering* 90, 1547-1560.

Liang, Y., S. Zhao, X. Jiang, X. Jia, and W. Li (2013). Numerical simulation on flow field of oilfield three-phase separator. *Journal of Applied Mathematics* 2013(2), 6 pages.

Shaban, H. I. (1995). A study of foaming and carry - over problems in oil and gas separators. *Gas Sep. Purif.* 9(2), 81-86.

Song, J. H., B. E. Jeong, H. J. Kim, and S. S. Gil (2010, May). Three-phases separator sizing using drop size distribution. In: *Offshore Technology Conference*, Houston, Texas, USA, paper 20558-MS.

Svrcek, W. Y. and W. D. Monnery (1993, Oct). Design two-phase separators within the right limits, *Chemical Engineering Process*, 53-60.

Talbi, K, Z. Nemouchi, A. Donnot, and N. Belghar (2011). An experimental study and a numerical simulation of the turbulent flow under the vortex finder of a cyclone. *Journal of Applied Fluid Mechanics* 4(1), 69-75.

Vilagines, R. D. and A. R. Akhras (2010). Three-phase flows simulation for imp roving design of gravity separation vessels. In: *SPE ATCE*, paper 134090-MS.

Viles, J. C. (1992). Predicting liquid re-entrainment in horizontal separators, *Journal of Petroleum Technology* 45(5), 405-409.

Yayla, S., K. Kamal, and S. Bayraktar (2019). Numerical analysis of a two-phase flow (oil and gas) in a horizontal separator used in petroleum projects. *Journal of Applied Fluid Mechanics* 12(4), 1037-1045.